AAS 15-619

ORGANIZING BALLISTIC ORBIT CLASSES AROUND SMALL BODIES

Benjamin F. Villac[*], Rodney L. Anderson[†], Alex J. Pini[‡]

Orbital dynamics around small bodies are as varied as the shape and dynamical states of these bodies. While various classes of orbits have been analyzed in detail, the global overview of relevant ballistic orbits at particular bodies is not easily computed or organized. Yet, correctly categorizing these orbits will ease their future use in the overall trajectory design process. This paper overviews methods that have been used to organize orbits, focusing on periodic orbits in particular, and introduces new methods based on clustering approaches.

INTRODUCTION

Past and present missions to small bodies, such as the NEAR Shoemaker, Hayabusa and OSIRIS-REx missions,[1] have used a multi-stage approach to methodically characterize the target asteroids before approaching their vicinity with more confidence.[2] This strategy addresses the large uncertainty in the close-proximity dynamical environment prior to the first encounter. In each phase, the dominant forces driving the dynamics change, and various models need to be selected in the trajectory design process. For example, far from an asteroid, simplified dynamical models (ranging from linearized dynamics to averaging methods) can be used to provide a global overview of the dynamics with sufficient accuracy.[3] As data is gathered and better approximations of the gravitational field are obtained, the spacecraft is transferred to regions closer to the body, where the non-uniform gravity and rotational state of the small body need to be taken into account. In this phase, the dynamics can be chaotic and present non-intuitive regimes of motion, which present both challenges in operating an actual spacecraft and opportunities to develop new mission concepts.[4]

While current missions have used active control (either low-thrust in the case of the DAWN spacecraft[5] or closed-loop control for final descent to the surface and touch-down events), the study of ballistic orbits near these primitive bodies is also expected to support the development of innovative mission concepts, such as automated long-term exploration or navigation beacons, small probe swarms with limited control authority, or simply the selection of relevant orbits for particular scientific observations. In particular, several classes of ballistic orbits have been analyzed in detail (e.g., terminator, ecliptic or libration point orbits) and provide insights into what can be expected around a generic small body. Yet, these classes do not cover all the possible regimes of motion that are relevant for exploring mission concepts, and the variety of small bodies often presents a challenge in organizing the orbit options at a particular target. In order to facilitate the understanding of these ballistic options, this paper reviews some of the ballistic orbit classification methods and explores new approaches that organize the dynamics around a small body based on user-defined criteria.

A significant amount of work has been conducted on the classification of asteroids and comets types and the characterization of their dynamics. Reference 6, for example, summarizes a variety of models and methods ranging from linearized models to averaging and periodic orbits. While some of these models provide a global overview of the dynamics when sufficiently far from the body or when only simplified model parameters are available, most of the methods provide an approximate, local view of the dynamics when in a region of a few radii of the small body. Sophisticated analytic models can also become as complex to analyze as the initial

[*]Pr. Systems Engineer, a.i.solutions, Inc., 10001 Derekwood Lane, Lanham, MD 20706
[†]Technologist, Jet Propulsion Laboratory, California Institute of Technology, 4800 Oak Grove Drive, M/S 301-121, Pasadena, CA 91109
[‡]Systems Engineer, a.i.solutions, Inc., NASA GSFC, B28 N278, Greenbelt, MD 20771

dynamics they approximate. Numerical and dynamical systems methods then become relevant in computing and organizing interesting orbits in such regimes of motion.

Periodic orbits, in particular, provide a fundamental class with well-established computational methods[7–9] that also support the design of transfers by invariant manifold or graph search techniques.[10] When the dynamics cannot be approximated by a time invariant or time-periodic system, the computation of quasi-periodic orbits and local semi-analytical simplifications might provide some insights.[11,12] While sound computational algorithms for these objects have been developed,[4,13,14] the actual application in a mission design context requires a good understanding of the underlying local dynamics (e.g., available periodic orbits in a simplified model) and some 'manual' oversight to converge or check the validity of a solution.

Other methods examine sampling of the phase space to overcome the sensitivity of the local approaches and support the understanding of the global overview. For example, chaoticity indicator techniques classify the orbit according to a notion of stability,[4,15] while Poincaré map techniques coupled with continuation methods have been used in the Circular Restricted 3-Body Problem (CR3BP) to analyze unstable resonant dynamics.[16–20] Further work in rendering these techniques more effective in a mission design context have used image processing algorithms to extract relevant regimes of motion.[21,22] Other techniques leveraged graph search methods to efficiently compute transfers.[10,23]

A common feature of these methods (whether explicit or not) is the creation of databases (sets) of orbits and the use of algorithms to classify and extract useful information about each orbit set. While several of these techniques do not rely on *a priori* simplified dynamics, the challenge from a user's perspective then lies in relating their concern about specific mission objectives to the various characterizations of these dynamics (such as terrain coverage, surface lighting conditions, or tracking geometry). In this case, periodic orbits have an advantage in providing more readily understandable sets of orbits at the cost of using simplified dynamics and the possibility of missing less intuitive solutions. This approach has notably been applied to the Earth-Moon system where the CR3BP serves as a good approximation of the dynamics in a large region of space, and databases of both periodic orbits and low energy transfers[24–28] have been developed for these cases.

This paper reviews and explores some of the methods highlighted above in the context of small body trajectory design. Focus is given to periodic orbit databases given their ease of use as test cases. The issues associated with the effort in creating such orbit sets, the exhaustive nature and ease of application of the methods, and the relation of the generated orbits to the realistic dynamics and mission design concerns are addressed. In particular, data clustering techniques (k-nearest neighbors and k-means algorithms) are explored as a tool to integrate several of the approaches mentioned above and provide a middle ground between optimization and flexible design space exploration. Testing of some of these methods (periodic orbits, Poincaré maps, random sampling and clustering) is performed in the context of the asteroids 25143 Itokawa and 2008 EV5 given their selections as misison targets. In particular, various models of the dynamical environment are considered with a focus on the Augmented Hill's 3-body Problem (AH3BP) and a uniformly rotating body.

SAMPLE ASTEROIDS AND DYNAMICAL MODELS

Before proceeding to the exploration of the dynamics and evaluation of orbit classification techniques, test cases must be defined. This section reviews selected asteroids and the relevant models used in this study. These include the AH3BP to approximate the dynamics at relatively large distances from the asteroid and a rotating spherical harmonic model for close proximity dynamics.

25143 Itokawa and 2008 EV5

The selection of a target asteroid in a space exploration context is often a problem in itself. Because of the scientific, commercial and technical reasons of asteroid exploration, some current endeavours have focused on smaller sized small bodies. In particular, Itokawa has already been visited by the Hayabusa mission and is being considered as a candidate destination for the Asteroid Redirect Mission (ARM) due to the presence of a precursor mission.[29–31] Additionally, EV5 is now the baseline target asteroid for ARM because of its suspected material composition.[29] Both of these asteroids are relatively small, yet possess different characteristics and have been used as drivers in exploring the organization of orbits around small bodies in general.

The orbital and physical characteristics of the selected asteroids are captured in **Figures 1-2**, and **Table 1**[*]. A notable difference between these two asteroids is the relatively circular orbit of EV5 compared to a significantly eccentric orbit for Itokawa. Still, these two bodies are both near-Earth asteroids that are orbiting the Sun within similar solar distances. The parameters for Itokawa are better known than those for EV5 given the previous visit to this body and thus provide an example where a more accurate model is available. Nevertheless, higher order models for EV5 are also available from distant observations and have been used as representative values for this case. For most asteroids, the uncertainties on the orbit, spin state and mass are quite significant, and the model parameters should be understood in this context.

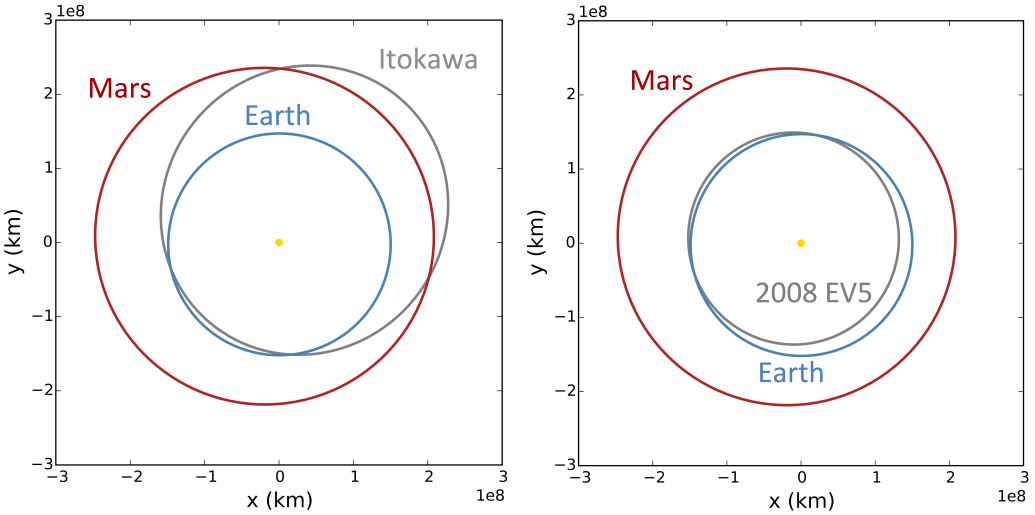

Figure 1. Illustration of Itokawa and EV5 Heliocentric Orbits.

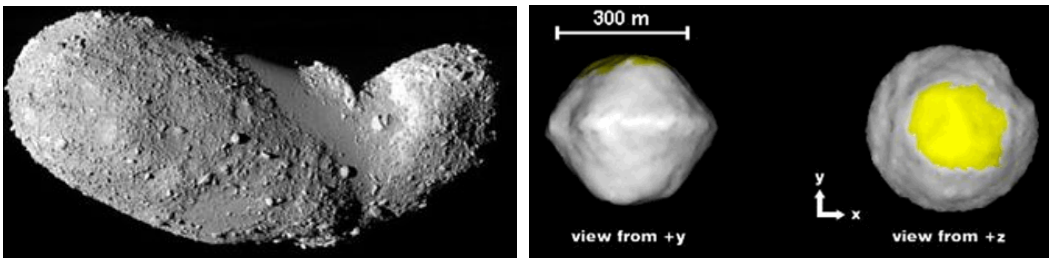

Figure 2. Illustration of Itokawa and EV5 Approximate Shape. Images courtesy of JAXA and NASA/JPL, respectively.

Table 1. Dynamical and physical parameters for Itokawa (from Ref. 32) and EV5 (from Ref. 33).

Parameter	Itokawa	EV5	Parameter	Itokawa	EV5
Eccentricity	0.280	0.084	μ ($\frac{km^3}{s^2}$)	2.36e-9	4.69e-9
Perihelion dist. (AU)	0.953	0.878	Grav. model radius (m)	400	202.607
Inclination (deg)	1.621	7.437	Rotation period (h)	12.132	3.725
Long. of asc. node (deg)	69.081	93.399	Pole Long. (deg)	0	180
Arg. of perhelion (deg)	162.810	234.803	Pole Lat. (deg)	-90	-84 $\pm$10

In addition to the asteroid parameters, the spacecraft properties should also be taken into account. Depending on the properties of the spacecraft, the gravitational attraction from the body can be smaller than the solar radiation pressure (SRP) at certain distances, as shown in **Fig. 3** below. The SRP is expressed here using a simple flat plate model, and depends on the area-to-mass ratio of the spacecraft. In order to select representative values, several past and current mission have been researched. In the case of the ARM mission,

[*]Numbers are rounded to the 3^{rd} decimal point.

the area-to-mass ratio for a recent baseline is approximately 0.028 $\frac{m^2}{kg}$ at the time of asteroid approach.[30] For missions, such as NEAR Shoemaker, Hyabusa, Dawn and Rosetta, estimates of area-to-mass ratio at the begining and end of the mission range within 0.014 to 0.057 $\frac{m^2}{kg}$ and in the following values within the range 0.01 to 0.06 $\frac{m^2}{kg}$ have been selected as representative spacecraft properties.

Beyond these physical parameters, the dynamics of an orbiter depend to some degree on the particular form of the model chosen, which depends in turn on the forces included in the dynamical model. In the case of an asteroid orbiter, these include the asteroid heliocentric model (mean circular or elliptic), the solar tide model, the small body gravitational field, the SRP and possibly other planets, tides, and spacecraft specific forces. As a first step in selecting a model, the relative forces of SRP and gravity have been explored.

Approximating the gravitational acceleration as that of a point mass and the SRP acceleration as a cannon ball model for several area-to-mass ratios, the expected orders of magnitude of the accelerations as a function of distance from the small body have been computed, as shown in **Fig. 3**. Further force comparison for EV5 is provided in Ref. 34, where similar results are obtained. In particular, it is observed that the gravitational acceleration is the dominant force only a few radii away from the body (10 radii for EV5 and from 3 to 7 in the case of Itokawa). Further out, the SRP and solar tides become dominant, and the non-uniform gravity field also becomes close to a point mass, leading to simplified dynamics represented as augmented restricted three-body problems. In regions close to the asteroid, the SRP force may be neglected in a first approximation, thereby representing the dynamics as a rotating non-uniform gravity field. These models are reviewed in the paragraphs below. The general case combines all these effects and becomes a more complex, time-varying model with dynamics dependent on the initial epoch chosen.

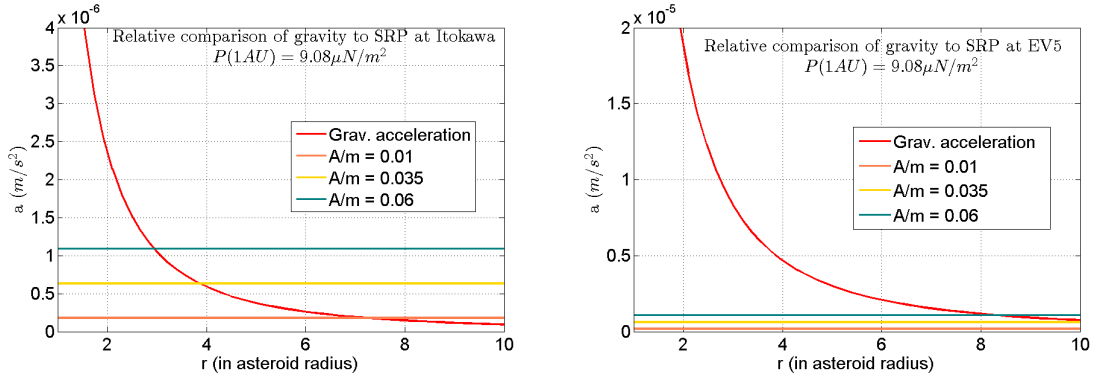

Figure 3. Comparison of SRP and Gravitational Accelerations. Left: Itokawa; Right: EV5.

Augmented Normalized Hill Three-Body Problem

The Augmented Normalized Hill Three-Body Problem (ANH3BP) is a simple dynamical model that captures the distant dynamics of an asteroid orbiter by including the solar tides, point mass gravity field of the asteroid and a simple flat-plate model for the solar radiation pressure. As in Hill's problem, the model is expressed in a synodic frame centered at the asteroid, and the Sun is taken to be at 'infinity' so that the solar radiation pressure direction is constant and along the frame x-axis. This model is representative of a class of distant dynamics models that include a form of the restricted three-body problem and SRP model.

The model can be expressed with an elliptic heliocentric orbit for the asteroid, but is often used as a local approximation with the small body orbit assumed to be circular. While this approximation may not be as justified for Itokawa as EV5, it provides a conservative model, whose Hamiltonian $\mathcal{H}$ is preserved along the motion of an hypothetical orbiter:

$$\mathcal{H} = \frac{1}{2}((p_x + y)^2 + (p_y - x)^2 + p_z^2) - \Omega \qquad \text{where} \qquad \Omega = \frac{1}{2}(3x^2 - z^2) - \frac{1}{r} - \beta x \tag{1}$$

Here x, y, and z gives the position in the rotating frame, and p_x, p_y, and p_z are the corresponding conjugate momenta. Then $r = \sqrt{x^2 + y^2 + z^2}$, and the normalized SRP acceleration, β, is given in terms of a flat plate

model:

$$\beta = C_r P_0 \frac{A}{mR^2} \left(\frac{L}{T^2} \right)^{-1}; \quad L = R(\tfrac{\mu_{ast}}{\mu_{sun}})^{1/3}; \quad T = \frac{1}{N}, \text{ with } N = \sqrt{\mu_{sun}/R^3} \tag{2}$$

where $P_0 = 9.56\mu N/m^2$ is the average solar flux at $1AU$ and R is the asteroid distance to the Sun in astronomical units. The reflectivity coefficient C_r and the area-to-mass ratio are used to scale the magnitude of the acceleration based on the spacecraft properties, while L and T are the physical units of length and time used to normalize the dynamics. The values of these units for Itokawa and EV5 are provided in **Table 2**. Note in particular, that the time scale is quite large compared with the rotation period of the asteroid, showing that the close proximity dynamics driven by the gravity field can be approximated by ignoring the motion of the asteroid around the Sun to first order.

Table 2. ANH3BP units of length and time for Itokawa and EV5.

Parameter	L (km)	T (days)	Normalized radius
Itokawa	51.679	88.51	7.74e-3
EV5	47.029	54.497	4.308 e-3

The Hamiltonian value expressed in position and velocity coordinates is also referred to as the Jacobi constant and is given as $C = \frac{1}{2}v^2 - \Omega$, where $v = |\mathbf{v}|$ is the magnitude of the dimensionless velocity. In particular, the conservation of this quantity implies the existence of zero velocity surfaces at a fixed C value, as for Hill's problem.

By evaluating the normalized SRP acceleration effects for the extrema area-to-mass ratios considered (0.01 to 0.6 $\frac{m^2}{kg}$) at periapsis and apoapsis of the asteroids' orbits, a range of β values from 27 to 511 was determined to encompass the dynamical environment about either body for a variety of spacecraft. That is, the results obtained for a particular value of β could be applied to either asteroid, assuming the visiting spacecraft had the corresponding A/m ratio to achieve that value of β. This is a large range of parameters and indicates the large variability in dynamical characteristics as different asteroids or spacecraft parameters are considered.

For example, **Fig. 4 (Left)** represents the variation of the x-coordinates of the two collinear equilibria present in the AH3BP for different values of β. As β goes to zero, we recover the two collinear Lagrange points of the Hill's problem. As β increases, the L_2 point approaches the center of the asteroid, while L_1 moves further away. The figure only shows a small range of β values outside of the region of interest, to indicate the scale of the movement of L_1 and L_2. For the largest β values considered, the L_1 point is quite far from the asteroid (several thousands of kilometers), while the L_2 point is quite close (a few kilometers). Note also the significant increase in the largest eigenvalue of the linearized dynamics at L_2 (**Fig. 4 (Right)**), showing the highly unstable character of the dynamics near the L_2 region; at these parameter values, the close and far dynamics are thus expected to interact strongly.

The model limitations should thus be kept in mind: as we approach the surface of the asteroid, the AH3BP is no longer a valid model, and the non-uniform gravity field of the asteroid then becomes dominant. Also, shadow effects are not taken into account here, so the actual L_2 location is only representative of a region where periodic orbits should exist rather than an actual point where a spacecraft would be placed.

Uniformly Rotating Gravity Field

At the other end of the model approximations, a uniformly rotating gravity field can be used to represent the close proximity dynamics of a small body orbiter. In the case of Itokawa and EV5, we have seen in **Fig. 3** that within a few asteroid radii, the gravitational attraction is the dominant force, so that SRP and solar tides can be ignored in a first approximation. However, as opposed to a planetary orbiter, the gravitational effects cannot generally be well approximated by a point mass or a very low order gravity field due to the unusual shapes of the asteroids.

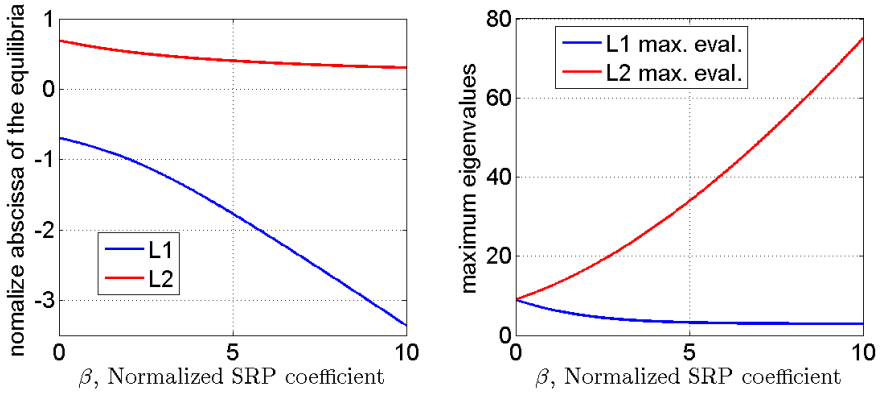

Figure 4. Abscissa of the Relative Equilibria of the AH3BP Model as a Function of β (Left) and Corresponding Extrema Eigenvalues (Right).

Several models can be selected for modeling the gravitational potential, such as mass concentrations or a polyhedral model,[35] a 'cube tree',[36] and elliptic or spherical harmonics, as chosen here. Whatever choice is selected, it should be recognized that none of these models represent the actual gravitational effects given the uncertainty in the model parameters prior to, or even during the encounter with such targets. However, basic assumptions and prior flight data provide an overview of the dominant features of the dynamics, as explored in the following paragraphs. In the case of EV5, an 8^{th} degree and order field has been used, while a 30×30 field is available for Itokawa. However, in that case, only a 16^{th} order and degree has been implemented.The gravitational potential is expressed in the asteroid body frame as:[37]

$$U(r,\lambda,\phi) = \frac{\mu}{r}\sum_{l=0}^{l_{max}}\sum_{m=0}^{l}\left(\frac{a_e}{r}\right)^l \bar{P}_{lm}(\sin\phi)(\bar{C}_{lm}\cos(m\lambda) + \bar{S}_{lm}\sin(m\lambda)) \tag{3}$$

where (r,λ,ϕ) represent the spacecraft distance, longitude, and latitude, a_e is the mean asteroid radius, $\bar{P}_{lm}$ is the normalized associated Legendre function evaluated for degree l and order m of the expansion, and $\bar{C}_{lm}$, $\bar{S}_{lm}$ are the corresponding normalized spherical harmonic coefficients.

Some of the asteroids present chaotic rotational motion, and a time-varying model must then be considered. In this case, the rotation axis of the asteroid is not fixed and the 'simplified' dynamical model can become as challenging to analyze as a more general model. Fortunately, the available data for the two asteroids considered in this paper suggests that they possess a relatively fixed rotational state, with the pole axis either nearly aligned or opposite the asteroid's heliocentric orbital angular momentum vector. This may be used to simplify the inclusion of the solar tides in the dynamics. However, in this paper, we consider only the effects from a rotating non-spherical gravity field as viewed from the asteroid body frame, neglecting SRP, solar tides, and the rotation of the synodic frame. The equations of motion are thus given as an autonomous Hamiltonian system, with Hamiltonian:

$$\mathcal{H} = \frac{1}{2}((p_x + \omega_{pole}y)^2 + (p_y - \omega_{pole}x)^2 + p_z^2) - \frac{1}{2}\omega_{pole}^2(x^2+y^2) - U(x,y,z) \tag{4}$$

where, U represents the gravitational potential described above and ω_{pole} is the scalar rotation rate of the asteroid around its pole. Similar models have been used to analyze some of the dynamics around 4 Vesta[4] and other larger asteroids, for example.

With this choice of the close proximity dynamics model, valid from a reference sphere bounding the asteroid to a few radii away from that sphere, the dynamics typically present several equilibria (analogous to the geosynchronous dynamics observed around the Earth). **Fig. 5** provides a graphical representation of these points within the non-uniformity of the gravitational potential. Interestingly, while appearing more spherical in shape than Itokawa, the model for EV5 leads to 6 equilibria, while Itokawa presents the more typical number of 4 equilibria.

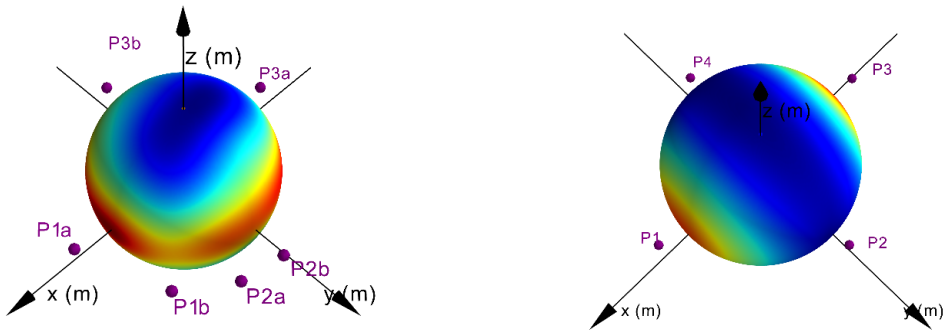

Figure 5. Left: Representation of EV5 Gravitational Potential with Relative Equilibria. Right: Similar Representation for Itokawa. The red regions indicate low potential values, while the blue indicates larger values. The axis are the body fixed axis associated with the spherical harmonic models used.

More General Dynamical Models

A more general dynamical model of an asteroid orbiter involves the inclusion of all the previously mentioned effects: a non-uniform, rotating gravity field, solar radiation pressure and tides, and elliptic motion around the Sun. Still, in this more general setting, the knowledge of (or trust in) the model parameters have to be balanced with the magnitude of some of these effects. For example, while the influence of other planets should be accounted for, it might be much smaller than the uncertainty on the SRP or gravity model. Also, the effects of shadows can be ignored in a first approximation if the motion is in a gravity dominated regime.

Regardless of the simplifications, the above model couples several natural frequencies (rotational vs. orbital period) and leads to a time varying dynamical system. In such a model, there is no conserved integral of motion and the spacecraft can move into different regimes of motion starting from the same initial condition at different epochs. The libration points present in the AH3BP are not necessarily approximately preserved for large area-to-mass ratios (we have seen that for large β values, the L_2 point is quite close to the surface, where non-spherical gravitational forces cannot be neglected). Periodic orbits also cease to exist, leaving the place to quasi-periodic orbits with slow and fast forcing frequencies. The interaction between the gravity field and SRP is notably expected to lead to highly chaotic dynamics, and it is unclear in general how closely approximate regimes of motion computed in the simplified models continue to represent the actual dynamics.

PERIODIC ORBITS AND ORBIT DATABASES

As mentioned in the introduction, a general method to explore the dynamics of an autonomous system consists of exploring the set of periodic orbits. This dynamical systems approach has been applied extensively in astrodynamics, and recent research has involved the development of databases of such orbits. While periodic orbits require the system to be time-invariant or time-periodic, the underlying regimes of motion captured in these particular solutions provide a template of the nearby dynamics. In this section, sets of periodic orbits are computed in the simplified models described in the previous section using two methods: one based on continuation and bifurcation analysis (referred to as the CBA approach) and the other using differential correction in conjunction with a random search over the set of symmetric orbits. These sets will then be used in the next section as test cases for the clustering methods.

The CBA Approach

The continuation and bifurcation analysis approach consists of starting from known solutions and numerically extending these by slowly changing their defining parameters. The most fundamental case consists of equilibria, for which linearized solutions are extended to the non-linear regime. General theorems support the existence of nearby solutions and thus the trust in the numerical output. In the case of periodic orbits, the

existence of the periodic orbit families around the equilibria mentioned in the previous section is guaranteed by the Lyapunov or Sternberg theorem, for example. Once a starting solution is found, pseudo-arc length methods can be used to continue the periodic orbit in a family of smoothly varying parameter, such as orbital period or energy. The method used in the following paragraph follows Reference 8 and used the AUTO continuation package.[38] Other solutions, such as quasi-periodic orbits, or stable and unstable manifolds, can also be continued from periodic orbits in many situations.

In the case of the AH3BP at $\beta = 27$ for example, **Fig. 6** presents a few orbits obtained from the continuation of the vertical Lyapunov orbits at L_2. It can be seen that these families can be extended quite far from the linear regime, up to impact with the small body or escape to infinity. However, the numerics are often very sensitive as the Lyapunov exponent of these orbits can also grow without bound. In particular, for the case of $\beta = 511$, vertical families could not be numerically continued from a linearized approximation.

The numerical evaluation of the monodromy matrix along each of the computed solutions also permits the detection of bifurcations. Singularities are detected as an increase in rank deficiency of the matrix used in the prediction step: instead of having a single direction of motion, a 2-dimensional (or higher) space is allowed to first order while keeping the periodicity conditions satisfied. In those cases, other families of periodic orbits appear to branch off the initial family. This is the case of the well-known halo orbits, which correspond here to the family of terminator orbits.[8] **Figure 6** presents several members of the terminator family for the case of $\beta = 27$, as well as the synthetic representation of the computed orbits as a bifurcation diagram that consists of the representation of each orbit by their periapsis position.

A similar approach has been applied to the rotating gravity field model starting from each of the equilibria that have been computed. As noted previously, the equilibria alternate between stable and unstable. Two families of periodic orbits are found around the unstable equilibria (a near planar and a mostly vertical family), while three families of stable periodic orbits are found around the stable equilibria (the long and short planar families and a vertical family). The analysis of these points thus follows the similar pattern of the collinear and triangular equilibria of the CR3BP. Sample orbits and bifurcation diagram are shown in **Fig. 6** (bottom plots), indicating the complexity of the orbit set in those cases.

A particular feature of small bodies such as those considered here is the closeness of the equilibria to the surface of the asteroid. As a result, the continuation of the families quickly encounters the convergence sphere of the spherical harmonic model. However, from a numerical viewpoint, the families can be continued 'sub-surface' and sometimes lead to other valid solutions not apparently connected with an equilibrium point. This characteristic also holds for other gravity field models that allow sub-surface gravity fields to be computed (e.g., polyhedral models). This phenomenon occurred for EV5 for the P1b short and long families. Other continuations lead to families connecting two equilibria, such as the short period family of P2a and the planar family of P2b. Sub-surface bifurcation points can also be computed and may potentially lead to other valid families. However, the CBA approach can quickly become unwieldy and lead to numerical difficulties in continuing some families.

The CBA approach features a sound theoretical basis and represents a fundamental dynamical exploration tool, but is often difficult to apply beyond the main families that start from equilibria. The bifurcation analysis can be implemented to detect multi-revolution branches, but is so far not an automated process. Associated with the theoretical foundation, the method directly organized the set of periodic orbits computed into families organized as the branches of a tree structure starting from equilibria. It thus provides a high level understanding of the orbit structure of a problem.

Random Searches

To palliate the difficulty in exhaustively searching for all the periodic orbits with a CBA approach, a grid search for periodic orbits can be performed. The methods implemented here are an extension of the techniques applied to the planar CRTBP in Anderson, Campagnola, and Lantoine[19] to search for symmetric resonant orbits with multiple intersections of of the x-z plane. The method has been applied with success in the simplified AH3BP models, as discussed in the following paragraphs, but it is more challenging to apply in the non-uniform gravity field model.

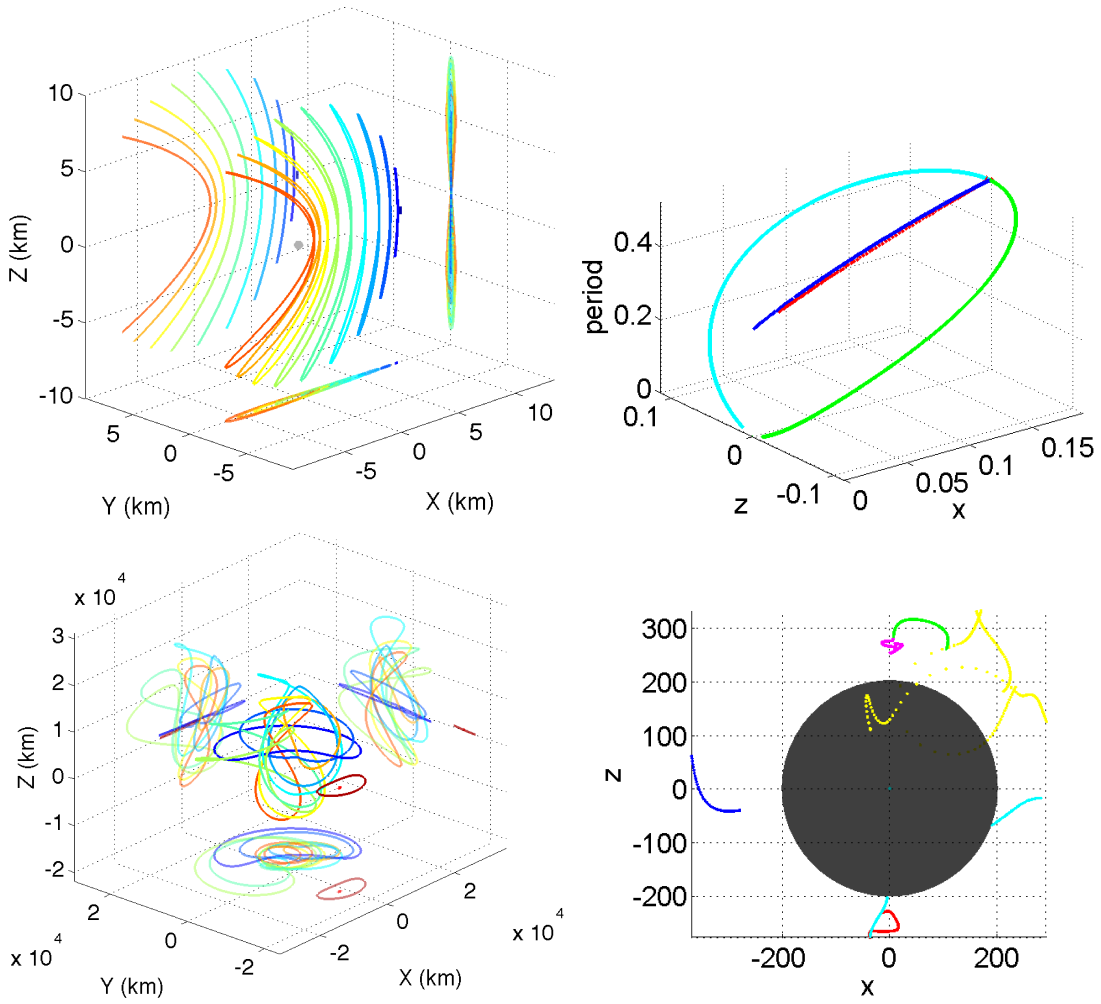

Figure 6. Example Periodic Orbits Around 2008 EV5 Generated Using AUTO. Top row: AH3BP for $\beta = 27$; L2 vertical family (left) and bifurcation diagram in terms of periapsis state and period (right). Bottom row: rotating gravity field. Sample orbit (left) and set of periapses of the planar (blue, cyan, green) and long period (red, magenta, yellow) orbits with convergence sphere of the model (grey).

Orbit Search in the AH3BP. A search was made for periodic orbits in the AH3BP using the symmetry about the x-z plane similar to the symmetry observed in the CR3BP.[39,40] Given this symmetry, if the tuple $(x, y, z, \dot{x}, \dot{y}, \dot{z}, t)$ represents a solution in the AH3BP, then the trajectories defined by the transformation $(x, y, z, \dot{x}, \dot{y}, \dot{z}, t) \rightarrow (x, -y, z, -\dot{x}, \dot{y}, -\dot{z}, -t)$ are also solutions of the AH3BP. The search was performed by setting up a grid of initial conditions for the spatial AH3BP as inputs to a single-shooting algorithm.[41] The algorithm for this case was modified to account for trajectories with multiple intersections of the x-z plane. The case described here was implemented for Itokawa with $\beta = 27$ where the initial C was varied from -35 to -10. A grid of initial conditions was defined in configuration space on the plane defined by $y = 0$ above the average radius of Itokawa $r_{itokawa} \approx 0.006534242$ LU. More specifically, the initial conditions are chosen with $-5r_{itokawa} \leq x \leq 5r_{itokawa}$ and $-5r_{itokawa} \leq z \leq 5r_{itokawa}$. The value for $\dot{y}$ on this grid was defined by the Jacobi constant according to

$$\dot{y} = \pm\sqrt{2\left(C + \frac{1}{r} + \frac{3}{2}x^2 - \frac{1}{2}z^2 + \beta x\right)}. \tag{5}$$

with $\dot{x} = \dot{z} = 0$. For this single-shooting algorithm, the values of z and $\dot{y}$ were allowed to vary to allow convergence on a periodic orbit with two perpendicular intersections of the x-z plane. **Figure 7** illustrates some of the points considered during the random search.

Poincaré maps provide one convenient method for visualizing the search space, and applying them to the planar AH3BP provides some additional insight into the problem. A set of initial conditions on $y = 0$ at $C = -7$ and $C = -10.3$with $\dot{y} > 0$ were used to generate the Poincaré sections shown in **Fig. 7**.

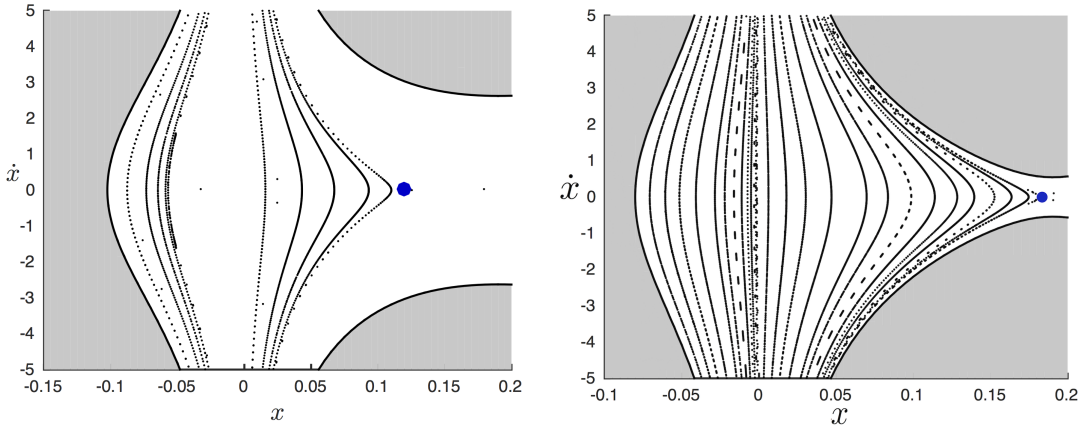

Figure 7. Sample Poincaré Maps for $C = -7.0$ (left) and $C = -10.3$ (right) in the Planar AH3BP for $\beta = 27$.

For these cases, a one-sided Poincaré map with $\dot{y} > 0$ was chosen. The forbidden region is shown in gray, and quasiperiodic orbits that remain near the asteroid may be observed in the resulting structure. The blue points correspond to periodic trajectories in the planar problem that were computed for the corresponding Jacobi constant. The trajectories are plotted in the x-y plane in **Fig. 8** for each of the Jacobi constants used in the Poincaré sections. Initial segments of the quasiperiodic orbits found in the Poincaré sections are also shown to illustrate the characteristics of these orbits. Note that they can come quite close to the center of the asteroid, but it is possible that segments of these trajectories or related trajectories may be useful for orbit design in some scenarios. A more detailed analysis of these types of trajectories will be made in the future.

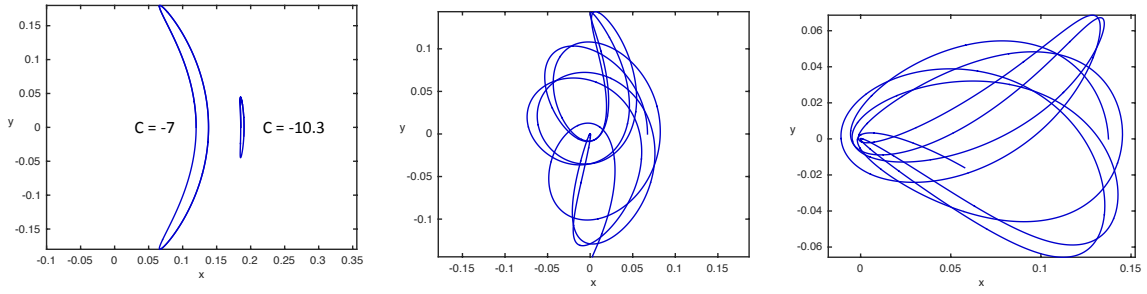

Figure 8. Sample Planar Periodic Orbits for $C = -7$ and $C = -10.3$ (left). Quasi-periodic Orbits from the Poincaré map at $C = -7$ (middle) , and $C = -10.3$ (right).

Although an initial Jacobi constant was selected for the single-shooting search algorithm, the final value was allowed to vary as needed by this algorithm, and the converged Jacobi constant was sometimes quite different. The algorithm also allowed the number of intersections of the trajectory to be varied as an input. For the results considered so far, the number of intersections were varied between 1 and 5. Note that the algorithm only differentially corrects orthogonal plane crossing, and as a result, it may compute either half or full orbits. If a half orbit is computed, the total number of intersections in those cases may thus be doubled. The period, final Jacobi constant, and maximum eigenvalue of the monodromy matrix were computed for later post-processing of the data.

Figure 9 (left) presents sample trajectories from this search, while the right plot shows the closest periapsis state for each periodic orbit found. As can be observed, the set of points is naturally organized around curves that would have been obtained had these orbits been computed with a CBA approach. This organization is especially the case for orbits of a given number of intersections, although several distinct curves are obtained even with such a number fixed. In any case, the grid search nature of the algorithm does not provide any immediate organization of the orbits obtained and the next section explores the use of clustering techniques to accomplish this task.

The application of the search and correction approach leads to new periodic orbits that were not found by a simple CBA. However, the sampling and exponential increase in computational cost, together with the sensitivity of longer period orbits, limit the number of orbits that can be obtained in this way. Further continuation of the obtained periodic orbits could provide a means to further refine some of this data set, but this has not been pursued given the sufficient number of orbits (about 2550) for testing clustering methods. In this case, however, the problem of merging common families can also be approached with clustering techniques, as discussed in the next section.

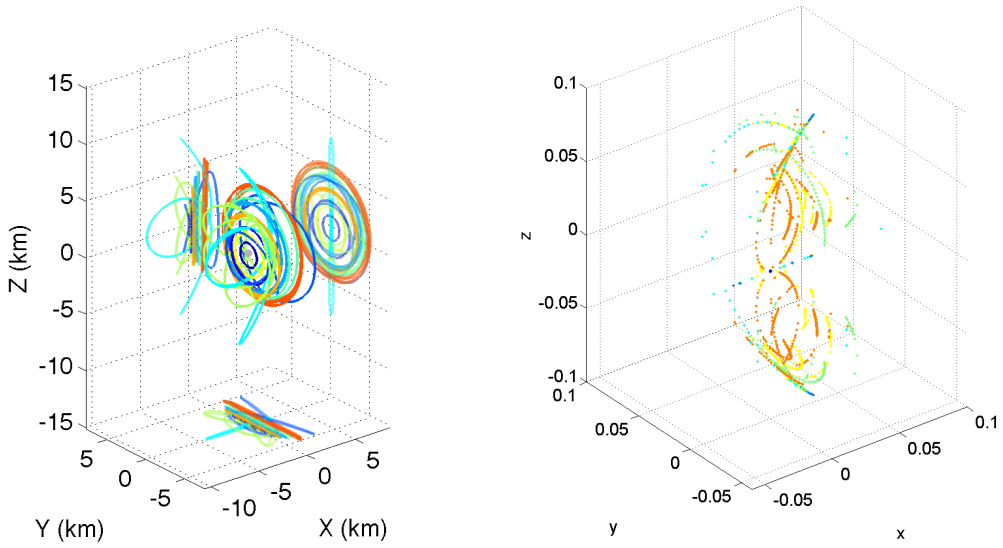

Figure 9. Left: Example of Periodic Orbits Found Using Random Sampling Technique. Right: Set of Closest Periapses of the Computed Periodic Orbits (colors are by intersection number).

Orbit Search in the Rotating Non-Uniform Gravity Field. Although continuation methods are able to compute many orbits of interest in the rotating non-uniform gravity field, an initial search was performed to search for orbits far from the body and near the x-y plane. A search for periodic orbits in this model presents several additional issues that are not present in models such as the AH3BP. In particular, the symmetry present in the AH3BP does not exist in this model, and the single-shooting method used previously is no longer applicable. There are two stages to this initial search as it is currently implemented. In the first stage, points on a grid in the x-y plane along $y = 0$ are selected. Then $\dot{y}$ values are selected in a range that produces trajectories that stay in the vicinity of the asteroid. An initial search is made to find trajectories that return to the initial point with similar velocities, and those that are within the desired tolerance are fed into a differential correction scheme. A multiple-shooting differential corrector was implemented to compute periodic orbits in this case[42] given the sensitivity of some of these orbits.

One of the difficulties that was encountered is that trajectories that initially appear nearly periodic may not converge to periodic trajectories through the differential correction process. Some of these trajectories that become nearly periodic have been retained for use in later trajectory design. Other trajectories do not converge to nearly periodic trajectories, and that set is discarded. These phenomena are inherent to the dynamics where the gravitational perturbations can be very small but lead to a multitude of local extrema for the differential correctors.

Orbit Databases

The previous results lead to sets of initial conditions that satisfy a periodic constraint and that are tagged by integers: branch number and solution labeling within a branch in the CBA approach, or the number of intersections in the random sampling search and correction approach. In particular, these integer tags represent an implicit organization of the set of orbits in terms of a database for which search and retrieval operations are then naturally associated. One can then search for orbits with a particular tag or set of tags.

However, while the search of a particular orbit with a given discrete tag value is relatively easy to achieve, more general criteria can be challenging to handle. For example, one can compute extra properties of the solution saved in the sets generated, such as the characteristic Lyapunov exponent of the periodic orbits, orbital period, Jacobi constant, or any other property of interest. These criteria are generally not integers, so the orbit selection problem becomes a multi-dimensional search problem. Therefore, a search for a set of orbits should then be considered as a search over ranges of parameters rather than the selection of a single orbit. In that sense, the search can be considered as a middle ground between optimization and approximations.

In particular, by considering more general sets of orbits, more complex classifications can be investigated. A simple case consists of a Poincaré map interpreted as a database of points: a random sampling of a Poincaré section and the recording of a (finite) sequence of subsequent intersections with each initial condition considered. In that case, one can look at extracting quasi-periodic orbits from this data set, for example.

More generally, with the above database of orbits, one can look at extracting particular features of the dynamics or classes of orbits that are relevant to a particular design context. As such, the search of the set of orbits becomes a classification problem that should be as flexible as optimization and allow for rapid evaluations of multiple options to perform preliminary trades without the cost of a full-blown optimization. This approach is addressed in the next section.

CLUSTERING ORBITS

Broadly defined, clustering refers to data mining techniques that aim at grouping sets of data with similar characteristics. Several general algorithms have been developed, but their applicability to orbit classification problems has not been investigated very deeply. Image segmentation techniques have been applied to 2-dimensional sets of initial conditions tagged by a scalar (color) and used to recover regions of quasi-periodic orbits.[21,43] However, more general problems such as the classification of a random set of periodic orbits in families, or the use of more general optimization criteria have not been considered. This section reviews some of the algorithms considered and discusses their applicability to orbital dynamics problems by considering two examples: the selection of observational orbits around EV5 and the organization of the periodic orbits computed into families.

Clustering Methods Overview

Several fundamental clustering algorithms have been developed for a wide variety of applications outside of astrodynamics. Given the focus of this paper only a subset of the approaches available have been considered as sample techniques of this general area of computer science. In particular, the k-means and k-nearest neighbors clustering techniques have been used as representative of two distinct classes of approaches. The following paragraphs provide a quick review of the underlying ideas for completeness. Further information on these approaches can be obtained from References 44 and 45, for example.

k-means Clustering. One of the fundamental clustering algorithms that has been used extensively is k-means clustering. This has been used in the context of image segmentation for stability region extraction in Ref. 43 and several heuristic approaches and implemetations to solve this problem are available. Given a set of N points in Euclidean space, $P = \{p_1, ..., p_N\}$ and an integer k representing the number of desired clusters to be computed, a k-means algorithm aims at finding k subsets of P, denoted $P_1, ..., P_k$, such that the average distances of the points to the barycenter of each subset set is minimized. That is, if $p_{i_1}, ..., p_{i_j}$ are the points with the subset P_i and b_i the barycenter of these points (as defined in the Euclidean space), then the average distance of the points can be computed as $D_i = \sum_{l=1}^{j} ||p_{i_l} - b_i||$ and the k-means problem is then to minimize $\sum_{i=1}^{k} D_i$ over the set of k subsets of P.

When formulated in this general context of an arbitrary set of points, the k-means problem cannot be solved in polynomial time on current computing architectures, but several heuristics exist. In particular, the iterative method of selecting an initial random set of subsets and assigning each point to the cluster with which its distance to the computed barycenter at the given step is smallest leads to fast convergence to local minima and provides good results for many applications.

Beyond the heuristic nature of the practical implementations, the k-means algorithm also assumes a Euclidean underlying metric between the points. A more flexible approach uses distances represented as normal probability distributions and leads to the expectation maximization problem. Given the scope of this initial study, this approach has not been investigated.

k-Nearest Neighbor Clustering. A different class of search algorithms consists of graph clustering algorithms. Here, a graph relating the various points is built from some condition and leads to clustering based on connected components or the extraction of subgraphs with a given connectivity number. Of particular interest for orbit classification is the k-nearest neighborhood graph formation approach. Here, each point (vertex) in the data set is linked to another point if the latter is within the k-nearest point on the whole dataset. That is, by computing the set of distances between each point, $d(p_i, p_j)$, the points $\{p_j\}$ can be ordered according to this distance from the vertex p_i and the first k such points are then connected to p_i. In the case of $k = 2$, we obtain curves, which is reminiscent of the organization of periodic orbits in branches. Other criteria in graph formation which represent distance can also be considered. In particular, a maximum distance can also be set as a connection criterion: link p_i to p_j if $d(p_i, p_j) < \epsilon$. This is the ϵ-neighborhood method and allows us to keep isolated solutions isolated.

In order to extract subgraphs, various techniques can be considered. The combination of k-nearest and ϵ-neighbors leads to disconnected components that can be used as a basic clustering method, as shown in the following paragraphs on the problem of random periodic orbits classification. More sophisticated techniques involve using the k-means algorithm to cluster the graph according to connectivity,[45] leading to spectral clustering methods. However, the balancing of the cluster size of these methods is not best suited here.

Other methods, such as support vector machines, can also be considered. A set of such algorithms has notably been implemented in the Matlab machine learning toolbox, thereby opening the way for easy acces to such techniques in orbital dynamics exploration. The issue, however, is in the problem formulation, set up, and defintion of relevant metrics, as is addressed in the following paragraphs.

Multi-Objective Exploration: An Asteroid Mapping Scenario

An example application of the k-means clustering technique operates on the previously computed periodic orbits in an attempt to identify attractive candidates for a high-fidelity asteroid characterization campaign. The extent to which the asteroid needs to be characterized is dependent upon the objective of the mission, but a CubeSat swarm or lander with limited control authority are examples of applications which may require an increased knowledge of the gravity field. Upon initial approach to an asteroid, the spacecraft will estimate critical asteroid parameters, such as spin and shape models, surface maps, and gravity models. Utilizing *a priori* information as an initial estimate, the determination of these parameters will be done in an iterative fashion, with the spacecraft gradually traveling closer to the asteroid and further refining the values.[2] A variety of trajectories can be utilized to accomplish this task, such as a terminator orbit,[46] near-inertial hovering,[47] or a series of hyperbolic fly-bys.[30]

However, this paper focuses solely on ballistic orbits bounded over a longer-term as a test case, and uses the periodic orbit databases described in the previous section. Among these ballistic orbits, some may be more favorable than others under a fixed set of mission constraints, such as hardware capabilities, operational schedule, and available time. Furthermore, the geometry and period of a particular orbit could be advantageous in terms of enabling the spacecraft to conduct the necessary actions to characterize the asteroid. Therefore, the clustering problem becomes one in defining metrics that are relevant for the problem and grouping the set of orbits with overall similar characteristics to enhance understanding of the design space.

General Considerations. A significant portion of the characterization process involves determination of the gravity field of the asteroid. As with geodetic satellites, an orbit designed to recover the asteroid's gravity

field should be selected to pass over as much of the body's surface as possible.[48] Because of this, geodetic satellites usually possess polar orbits which have short orbital periods relative to the rotational period of the Earth. This causes the satellite to experience gravitational effects from many regions of the Earth as the Earth rotates beneath it, providing a holistic representation of the Earth's gravity field. In order to map an asteroid's gravity field in the same manner, a similar orbit with widespread ground coverage is desired.

An important distinction between mapping Earth's gravity field and a distant small body's field is that the spacecraft rely on different measurement types to conduct the orbit determination necessary for gravity recovery. Geodetic satellites have a variety of measurement sources (such as GPS, low-low satellite ranging,[49] and a slew of data types from ground stations) that can present a data-rich environment with nearly continuous observations. A satellite orbiting an asteroid has more limited options for observations, including optical navigation, LIDAR, and occasional DSN passes. As a result, special consideration must be paid to achieving favorable lighting conditions, as camera imagery in the visible spectrum will likely play an integral part of the orbit determination process for any satellite visiting an asteroid.

Current optical navigation techniques utilize a series of images of the asteroid's surface to ascertain the spacecraft's relative state. This is achieved by correlating landmarks in surface images from a variety of spacecraft vantage points and/or lighting conditions to those in a previously constructed digital elevation model, obtained via stereophotoclinometry.[50] Both the map generation and relative optical navigation rely on the ability to obtain images of illuminated surface features and the shadows they cast, so an ideal characterization orbit would have substantial arcs where sufficient imagery could be gathered.

In addition to dense surface coverage and an abundance of time in illumination, stability is another desirable trait of a ballistic characterization orbit. A stable orbit (or relatively less unstable orbit) tends to require fewer stationkeeping maneuvers, which could lead to lower fuel consumption and also ease the operational burden.

Multi-Objective Formulation. The traits of an effective high-fidelity characterization orbit discussed above can thus be distilled into three criteria: terrain coverage, time in illumination, and stability. Each of these criteria can be represented by a user-defined metric; when these three metrics are calculated for each orbit in a set, they become the values that the k-means algorithm operates on to assign the orbits to clusters. Since the clustering metrics are defined at the discretion of the user, the k-means algorithm will produce results that correspond to the manner in which the inputs are formulated. Counter-intuitive outputs may thus be due to both the inputs or the clustering metrics definition.

The following multi-objective clustering test case is illustrated for the set of periodic AH3BP orbits with $\beta = 27$ identified using the random sampling technique described previously. A terrain coverage metric to distinguish between orbits with sparse and dense coverage could be related to their respective ground tracks on the asteroid itself. By dividing the surface of the asteroid into $n \times n$ degree bins and logging the amount of unique bins that were 'hit' by the ground track for a particular orbit, a measure of terrain coverage is obtained. For this study, n was selected to be 2 degrees and the asteroid was modeled as a sphere with the reference radius and spin state of 2008 EV5. To accurately assess the coverage for a particular trajectory, it needs to be propagated through the entire orbital period to ensure that the full range of geometry is realized. However, since the orbital periods in the data set vary greatly, trajectories with longer periods would likely encounter more unique bins, so the metric is normalized to be the number of unique bin hits per hour.

To quantify an orbit's ability to conduct surface mapping and optical navigation, a region of permissible lighting conditions was established. Assuming one image is taken every minute, the averaged number of useful observations per hour throughout the duration of each orbit was calculated. Useful observations were identified as occurring whenever the angle made between the Sun, asteroid, and spacecraft was between +/- 60 degrees, as specified by the ARM mission.[30]

In time-invariant systems, stability of periodic orbits is often evaluated based on the eigenvalues of the monodromy matrix. To reduce the multiple eigenvalues for each orbit down to one parameter for comparison with the rest of the set, the maximum real eigenvalue from each orbit was selected. This value, with higher numbers corresponding to higher instability, is the third and final metric around which the k-means algorithm identifies clusters for this study.

Results and Discussion. The top left panel in **Fig. 10** represents the results of the k-means clustering algorithm in graphical form. Each point on this plot represents a single orbit in the random sampling set, with Cartesian components corresponding to the three clustering metrics defined earlier. The locations of the points in 3-D space are determined before being passed to the k-means algorithm, which groups them into clusters having similar properties. The color of the point corresponds to the cluster that the point is assigned to; that is, points with the same color were identified by the k-means algorithm as having similar traits. Intuitively, the orbits that are more suitable for high-fidelity characterization are located in the 'top-right' corner of the x-y plane, having a dense ground track coverage, ample opportunity for visible camera imagery, and a low maximum real eigenvalue. The most attractive cluster is likely the cyan group in this case, as the orange group has denser ground track coverage but no illumination, lacking opportunities to do orbit determination via optical navigation. In essence, the clustering algorithm successfully organized two similar groups of orbits into different clusters for further investigation, indicating there are groups of motion possessing similar orbit characteristics.

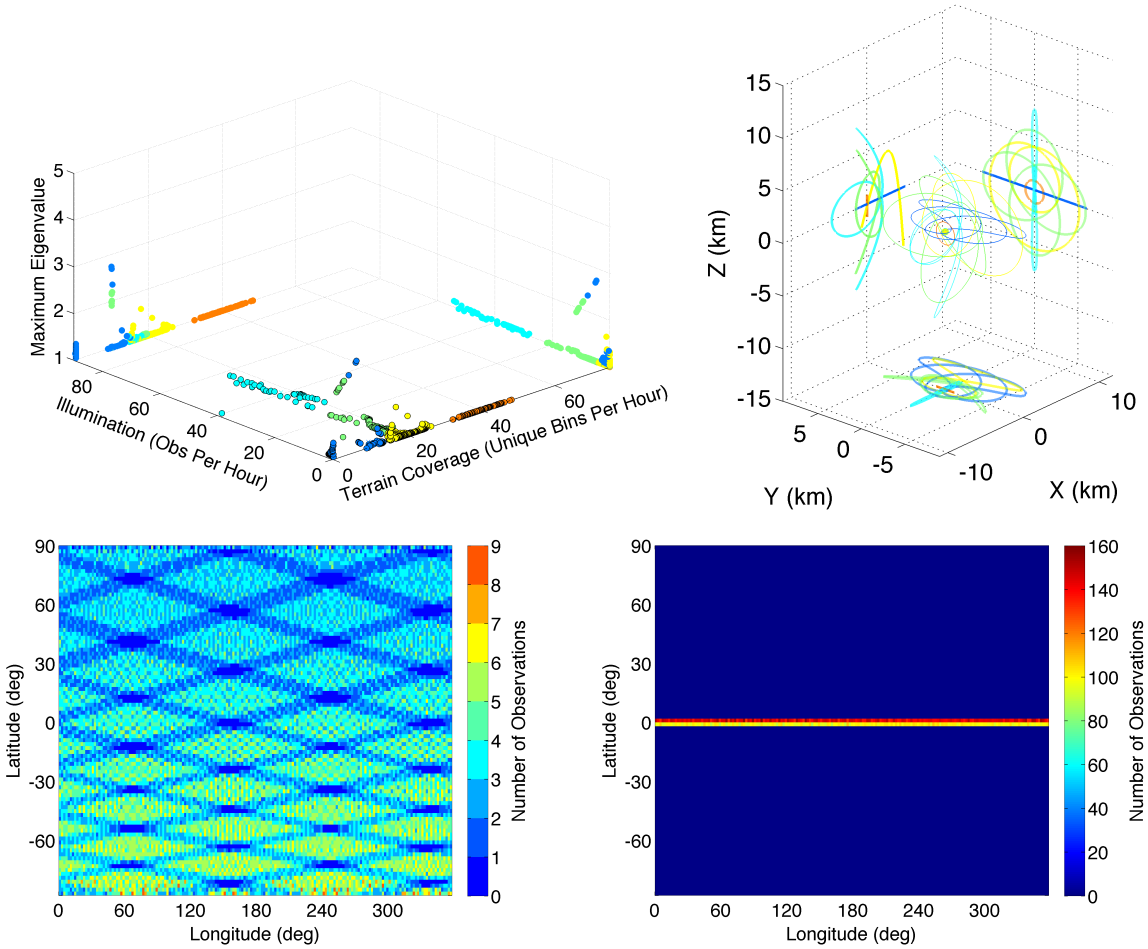

Figure 10. Clustering Results for Periodic Orbit Set Obtained Using Random Sampling Technique (as described in an earlier section). These orbits are in the vicinity of 2008 EV5 and assume AH3BP dynamics with $\beta = 27$. Top left: All orbits in the set grouped by cluster (color), as identified by the k-means algorithm. Top right: Representative orbits from each cluster. Bottom left: Example ground track corresponding to most dense cluster of orbits. Bottom right: Example ground track coverage from the most sparse cluster in the set.

The top right plot in **Fig. 10** shows an example orbit from each of the clusters identified by the k-means algorithm. The ideal characterization cluster (cyan) appears to be a family of vertical orbits, spending considerable time in a sweet spot a few km from the asteroid with sun-lit observations. Furthermore, the geometry

of this orbit is somewhat similar to that of a terminator orbit, in that the asteroid rotates beneath the spacecraft as it stays in roughly the same plane in the rotating AH3BP frame. This leads to dense ground track coverage, bolstering the orbit's attractiveness for characterization. Another interesting option is the green family of orbits that have several 'petals', which provides out-of-plane observations, but with fewer opportunities for valid surface imagery. As anticipated, the representative orbit in the orange family is a terminator orbit, which is analogous to a geodetic satellite's polar orbit in that it covers much of the surface quickly. However, the dynamics in this environment (namely SRP) cause the terminator orbit to reside entirely in darkness, causing it to be unsuitable for characterization.

The bottom two plots of **Fig. 10** show the observations of a nadir-pointing camera on the surface of a spherical asteroid, which is essentially equivalent to the ground track. For comparison purposes, the two orbits were propagated for the same amount of time (the longer of the two orbital periods) to illustrate the spatial distribution of observations in a fixed time span. The bottom left image corresponds to the orange terminator orbit family, which results in a nearly uniform coverage over the surface of the asteroid. On the opposite end of the spectrum, the bottom right image illustrates the spatial coverage offered by the dark blue planar orbit, which resides strictly in the latitude band of +/- 2 degrees. There are many observations near the equator, but for a nadir-pointing camera having characterization duties, this orbit is less than ideal.

Assessment of k-means Algorithm Performance. The above example illustrates some of the benefits and limitations of the clustering approach in the context of an orbit selection problem. In actuality, the desirable properties can be formulated as an optimization problem and could in principle be solved using an optimizer. However, the orbit set that was an input to the clustering algorithm was precomputed to satisfy a particular criterion. The clustering provided groups of orbits with similar properties. In particular, while the clustering is based on Euclidean distance and thus compounds all the characteristics used in a single number (when comparing between points), it does not reduce the problem to a single cost function. If a cost function was used, unrelated orbits could possess a similar performance index when measuring the norm of the vector formed by the 3 characteristics considered. Rather, the grouping via clustering is performed based on similarity among the points. The grouping in particular allows the user to refine an interesting set of options and reduce the search space to use in an optimizer.

Another interesting feature of the algorithm is the applicability with a larger set of metrics; that is, to work with n-dimensional measures of performance. For example, further analyses could aim to increase the fidelity of a particular characterization campaign if mission-specific parameters are known: if camera specifications and limitations are defined, then a minimum and/or maximum radius for allowable observations could be incorporated, as well as camera fields of view. Also, some knowledge of the capabilities of the terrain relative navigation algorithm could also be factored into the pre-processing for the clustering algorithm, resulting in a solution or observation 'quality' metric. Thus, a refinement or increase in the number of the performance metrics that are calculated for inputs to the k-means algorithm could be utilized to better represent the desired conditions for high-fidelity characterization. This aspect illustrates the potential of clustering algorithms for multi-objective problems' investigation in reducing the search space which is often expensive to characterize with optimization techniques, such as Pareto front computations over a large domain.

However, the experience with the above example indicates some challenges in using clustering and the k-means algorithm in particular. The heuristic used proceeded from a random sampling of the initial guess, which led to some variability in the clustering, with some cases of non-intuitive clusters. Here the limitation is in the particular implementation, and other implementations or techniques might be more efficient. Further investigation may aim to investigate the use of expectation maximization techniques as a better alternative to k-means. With toolboxes, such as the Matlab machine learning toolbox, the availability of multiple algorithms might provide a mission designer with an interesting tool to explore the design space.

While the application of the clustering algorithms is not overly computationally expensive, it should be re-emphasized that the main cost is in setting-up a relevant orbit database, defining the measures of performance and evaluating those on the desired set. This is a non-trivial effort when starting from scratch, but is reusable for a multitude of mission objectives and targets once in place. In the case of the k-means approach, the number of clusters k to use is not user-defined and several trials need to be performed to extract useful

clusters. This process can be somewhat automated by comparing the clusters obtained with increasing k or using a different method. This algorithm flexibility is not an advantage in the case considered, but has the benefit of being rather fast to compute once all the data has been generated.

Organizing Periodic Orbits

While the previous scenario looked at orbit classification from the viewpoint of multi-objective measures, a second class of problems consists of recovering known structures from an unstructured data set. A case in point is the recovery of periodic orbit families from the data sets generated by the search and correct method. The following paragraphs examine the use of graph clustering methods to perform such a task.

Orbit Families as Curves As discussed in the CBA approach section, periodic orbits in conservative systems are organized in a one-parameter set of orbits (families or branches), these sets being themselves organized (locally) as a tree structure. In particular, a set of parameters, such as the closest periapsis state and the orbital period, can be used to represent these curves in a parameter space*. In as much as the computed set is a discretization of such curves, the points on a periodic orbit branch are organized sequentially and thus connected to 2 neighborhood points. This suggests applying a 2-nearest neighbor graph formation method on the data set generated by the search and correct approach in the AH3BP.

As a first step, however, the set of orbits generated with the CBA approach in the AH3BP ($\beta = 27$) has been used to test the approach. The families of orbits are indeed known in that case and the ability of the method to separate branches can be tested there. To apply a 2-neighbor method, a distance must first be defined. In the following, the norm of the difference between the closes periapsis states of the orbits scaled by the period difference and velocity angles has initially been used:

$$d(\boldsymbol{X_i}, \boldsymbol{X_j}) = ||\vec{r_i} - \vec{r_j}||(1 + |T_i - T_j|)(1 + sin\angle(\vec{v_i}, \vec{v_j})) \tag{6}$$

While a full state norm can also be considered, the varying order of magnitudes between position and velocity led to defining the above metric. One could also use the value of an integral of motion in the definition. The above definition captures a notion of closeness used in the representation of the bifurcation diagram of **Fig. 6** and is physically intuitive. Orbits are close if their periapses, periods and velocity angles are close. However, the representation of an orbit as a single state limits the accuracy that can be expected from such distance functions, irrespective of the form of the function used, as discussed below. Alternatively, one can use an inverse distance or scaling law, such as $\exp(-d(\boldsymbol{X_i}, \boldsymbol{X_j})$, in building a graph (inverting the linking conditions inequalitites). The resulting form of the adjacency matrix results indeed the extracction of the graph connected components as a null space analysis of the graph Laplacian matrix.[45] This exponential transformation, referred to as a similarity condition, has been used in the following.

With this measure, each family (e.g., the L2 family) can be organized in the graph, with points having the closest distance from each vertex are connected. **Figure 11** (left) presents the results applied to each families computed and indeed results in a bifurcation diagram similar to the one presented in Fig. 6, with the planar and vertical L2 families having very close characteristics in this periapsis viewpoint. Upon closer inspection, however, each branch appears to consist of several disconnected components. In particular the number of connected components can be quite large overall, as shown in **Fig. 11**(right). This phenomenon is due to the non-uniform sampling of the families (notably of the L2 family which has been computed in several segments): two closest points may be on the same 'side' of the curve for a given vertex. This phenomenon can be eliminated by considering larger k values or adding a condition on the angle between successive neighbors. In particular, as shown in **Fig. 11** (right), the number of disconnected components reduces with increasing k. The graph 'curve' obtained may have multiple overlap, but the clustering of a family as one set of orbits is recovered. This can also be interpreted as a clustering of the 2-neighbor cluster themselves, by linking the closest end points together.

*The use of the period in particular is relevant in avoiding the intersection of period doubling families when they reduce to an orbit with apparently 1/2 of the period.

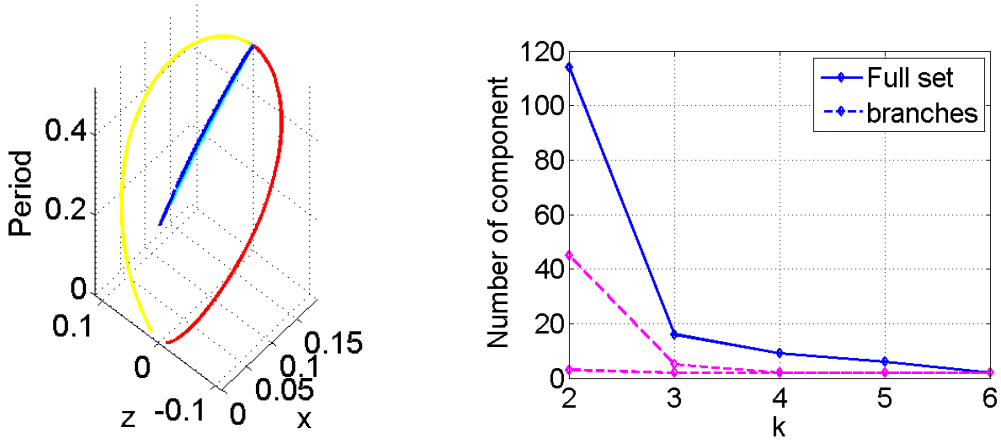

Figure 11. Individual Branch Clustering with a 2-Neighbor Approach. Left: AH3BP families ($\beta = 27$). Right: Number of connected components as a function of k.

Separating families A more interesting problem consists of separating the number of different families. Here, the k-neighbor graph formation is applied to the whole set of initial conditions generated without the a priori knowledge of the branch structure (i.e., all the branches are merged). A quick inspection reveals that the main families are indeed separated, but the planar and vertical families (which present very similar periapsis locations and periods) are not. A different choice of distance function (using the sum of closest periapsis and apoapsis positions instead of just the periapsis data as previously) allows however to easily separate the families. These results are shown in **Fig. 12** and illustrate some of the limitations of the approach: clustering does not replace the user understanding in defining appropriate metrics and set representation. In particular, one can expect as good a result as the parameterization of the orbit states distinguishes between the desired characteristics. These results also illustrate the benefit of using a priori information on the orbit set structure.

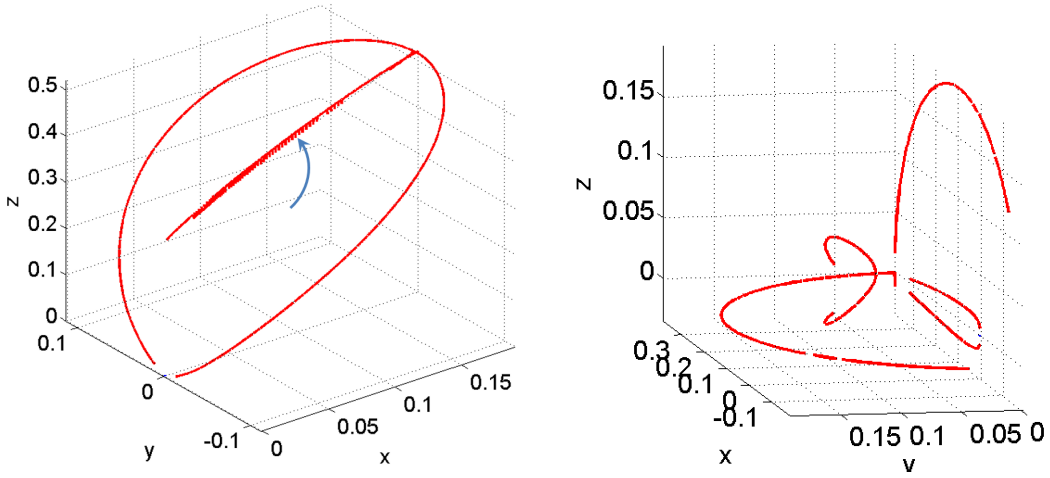

Figure 12. Full Set Clustering with a 2-Neighbor Approach (applied to the the L2 Families of the AH3BP, $\beta = 27$). Left: Periapsis parameterization with arrow indicating poor clustering of the Lyapunov and vertical families (compare with Figure 11 blue and cyan colors). Right: Addition of apoapsis data, the axes are the components of the sum of the closest periapsis and apoapsis states.

Besides these drawback, the method can be applied to the random set with interesting results as shown in **Fig. 13**, where data points are colored by number of intersection. As in the previous examples, the algorithm clusters some of the points incorrectly (notably the cyan colors), but connects many of the visually apparent components. This is the case notably for the densely sampled sets (green and organe), indicating that the

continuation of the random search solution woul dhelp in the clustering of the results as well (since it would results in denser set of point, albeit not organized, within a branch). The graph clustering approach thus leads, as for the previous example, to individual sets of orbits that share some common features. Each set is then available for further analysis.

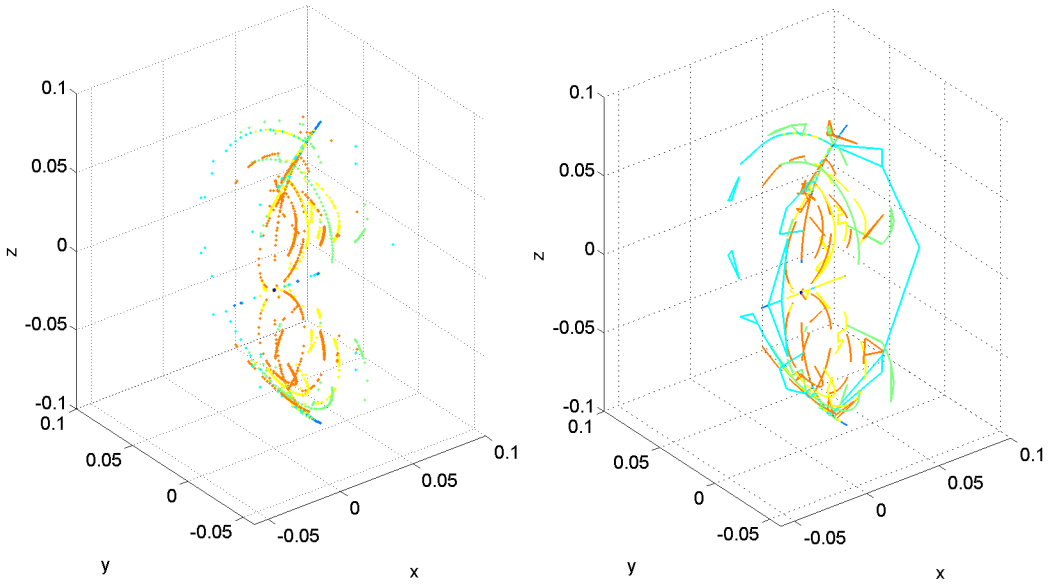

Figure 13. Graph Clustering Database of Periodic Orbits in the AH3BP. Left: Raw data set organized by intersection level. Right: Clustered graph by intersection level.

The above examples illustrates some of the interesting features of clustering methods as well as their inherent limitations and role of the user in applying those techniques to a particular problem. In particular, clustering provides an automated means of filling in the gap between a large dataset and the selection of orbits with particular properties and providing an ordering of the sets into smaller components that can then be analyzed individually. However, the graph method still requires the definition of appropriate metric for the data set considered. In the case of periodic orbits, branch segments of periodic orbits could be recovered, even though mis-classification also occurs due to sampling and particular choice of metrics. Further investigation will look at the continuation of the initial conditions obtained from the random search as a means to provide a denser set. As mention above, the issue of merging the data sets would then be addressed by the clustering approach presented. The development of further metrics of the quality of clustering would also be desirable to explore for a more quantitative analysis of the results obtained.

CONCLUSIONS

The presented research investigated the use of clustering as a ballistic orbit classification tool and the effort in generating relevant database of orbits for orbiters of small sized asteroids. Sample test cases of the approach have been investigated in the augmented Hill's problem and a rotating spherical harmonic gravitational field modeling the dynamics of an orbiter around EV5 or Itokawa. In particular, structured and unstructured databases of orbits have been generated. In the continuation and bifurcation approach, a limited set of periodic orbits is obtained with a clear structure of branches and linear order within a branch. In the case of random search and correct, the orbits are themselves constrained to be periodic, but lack the organization of the continuation approach. This case indicates that a larger range of motions is captured, at the cost of losing some of the informational organization and incurring a larger computational burden (though with a reduced setup and interaction cost on the user). In the more challenging cases, the correction approach also shows its limitation stemming from enforcing a particular constraint on the orbits which may not be appropriate for the particular dynamics considered. Thus, in the more general case, random sets of points (used for example in generating Poincaré maps) can be generated inexpensively, but without any immediate structural information that can separate the data into relevant sets for a particular application.

The set of techniques referred to as clustering have then been investigated for their potential to palliate the lack of organizational data and create groups of points with similar characteristics. A k-means approach has been applied to the case of an asteroid mapping scenario when a multi-objective problem is naturally present. The clustering approach does play the role of a pruning method to group orbits into user defined criteria. Each cluster can then be used for further analysis or start an optimization process. In particular, even though clustering algorithms are often formulated as optimization problems, they should not be considered as such for orbital analysis purposes. Rather, they can provide another tool for the analyst to use in exploring non-intuitive regimes of motion as can be found around small bodies. The data within a cluster can then be used to bound the search domain of an optimizer.

Another approach based on building graphs connecting nearby points within the generated set of orbits and extracting connected components is shown to provide a tool to re-organize a set of periodic orbits into similar structures as the continuation and bifurcation approach. The method still requires some user input in defining the correct measures of distance and representation of the dataset. As for the previous example, clustering thus appears as a tool to facilitate the organization of a large set of data into classes of motion that share similarities, but does not replace the user understanding in defining relevant classification criteria.

The results presented in this paper illustrate some of the challenges in both creating relevant orbit set and organizing those within the context of small body orbiter missions. However, these results are exploratory in nature and need further investigation. The particular algorithm best suited for the purpose considered, the quantification of the clustering quality and the further investigation of classification of particular types of motion, such as quasi-periodic orbits have not yet been addressed. With the availability of clustering algorithms libraries, such as the matlab machine learning toolbox, the use of clustering in orbital analysis may provide an interesting complement to the current approaches in mission design and concept exploration.

ACKNOWLEDGEMENTS

This research has been sponsored by the AMMOS technology development task. A portion of the research presented in this paper has been carried out at the Jet Propulsion Laboratory, California Institute of Technology, under a contract with the National Aeronautics and Space Administration.

REFERENCES

[1] D. S. Lauretta and the OSIRIS-REx team, "An Overview of the OSIRIS-REx Asteroid Sample Return Mission," 43rd Lunar and Planetary Science Conference, No. 2491, 2012.

[2] J. K. Miller, A. S. Konopliv, P. G. Antreasian, J. J. B. S. Chesley, C. E. Helfrich, W. M. Owen, T. C. Wang, B. G. Williams, D. K. Yeomans, and D. J. Scheeres, "Determination of Shape, Gravity, and Rotational State of Asteroid 433 Eros," Icarus, Vol. 155, No. 1, 2002, pp. 3–17.

[3] D. J. Scheeres, "Satellite Dynamics About Asteroids," Spaceflight Mechanics: Proceedings of the AAS/AIAA Spaceflight Mechanics Meeting held February 14-16, 1994, Cocoa Beach, Florida (J. John E. Cochran, J. Charles D. Edwards, S. J. Hoffman, and R. Holdaway, eds.), Vol. 87 of Advances in the Astronautical Sciences, San Diego, California, American Astronautical Society, Univelt Inc., 1994, pp. 275–292.

[4] J.-M. Mondelo, S. B. Broschart, and B. F. Villac, "Ballistic Transfer Across the 1:1 Resonance Around Vesta Following Invariant Manifolds," Journal of Guidance, Control, and Dynamics, Vol. 36, July–August 2013, pp. 1119–1133.

[5] M. D. Rayman, T. C. Fraschetti, C. A. Raymond, and C. T. Russell, "Dawn: A Mission in Development for Exploration of Main Belt Asteroids Vesta and Ceres," Acta Astronautica, Vol. 58, No. 11, 2006, pp. 605 – 616.

[6] D. J. Scheeres, Orbital Motion in Strongly Perturbed Environments: Applications to Asteroid, Comet and Planetary Satellite Orbiters. Berlin Heidelberg: Springer Praxis, 2012.

[7] S. B. Broschart and B. F. Villac, "Identification of Non-Chaotic Terminator Orbits Near 6489 Golevka," Spaceflight Mechanics: Proceedings of the AAS/AIAA Space Flight Mechanics Meeting held February 9-12, 2009, Savannah, Georgia (A. M. Segerman, P. C. Lai, M. P. Wilkins, and M. E. Pittelkau, eds.), Vol. 134 of Advances in the Astronautical Sciences, San Diego, CA, American Astronautical Society, Univelt Inc., 2009.

[8] K. Liu and B. Villac, "Periodic Orbit Families in the Hill's Three-Body Problem with Solar Radiation Pressure," AAS Spaceflight Mechanics Meeting, No. AAS 10-118, Irvine, California, February 14-17 2010.

[9] D. G. Yárnoz, D. J. Scheeres, and C. R. McInnes, "On the a and g Families of Symmetric Periodic Orbits in the Photo-Gravitational Hill Problem and Their Application to Asteroids," AIAA/AAS Astrodynamics Specialist Conference, No. AIAA 2014-4119, San Diego, California, August 4-7 2014.

[10] E.Arnal Fort, B.Villac, J-M.Mondelo, "Exploration of a Graph Based Method for Orbital Transfers near Small Bodies," 2013 AAS/AIAA Astrodynamics Specialist Conference, No. AAS 13-81, 2013.

[11] S. B. Broschart, G. Lantoine, and D. J. Grebow, "Characteristics of Quasi-Terminator Orbits Near Primitive Bodies," Spaceflight Mechanics: Proceedings of the AAS/AIAA Spaceflight Mechanics Conference August held February 10-14, 2013 in Kauai, Hawaii (S. Tanygin, R. S. Park, J. Thomas J. Starchville, and L. K. Newman, eds.), Vol. 148 of Advances in the Astronautical Sciences, San Diego, California, American Astronautical Society, Univelt Inc., 2013, pp. 953–968.

[12] G. Lantoine, S. B. Broschart, and D. J. Grebow, "Design of Quasi-Terminator Orbits Near Primitive Bodies," AAS/AAIA Astrodynamics Specialist Conference, No. AAS 13-815, Hilton Head Island, South Carolina, August 11-15 2013.

[13] Z. Olikara and K. Howell, "Computation of Quasi-Periodic Orbit Invariant Tori in the Restricted Three-Body Problem," AAS Spaceflight Mechanics Meeting, No. AAS 10-120, West Lafayette, Indiana, February 14-17 2010.

[14] P. G. Egemen Kolemen, N. Jeremy Kasdin, "Multiple Poincaré sections method for finding the quasiperiodic orbits of the restricted three body problem," Celestial Mechanics and Dynamical Astronomy, Vol. 112, 2012.

[15] Benjamin F. Villac, "Using FLI Maps for Preliminary Spacecraft Trajectory Design in Multi-Body Environments," Celestial Mechanics and Dynamical Astronomy, Vol. 102, No. 1-3, 2008, pp. 29–48.

[16] R. L. Anderson and M. W. Lo, "Flyby Design using Heteroclinic and Homoclinic Connections of Unstable Resonant Orbits," Spaceflight Mechanics: Proceedings of the 21st AAS/AIAA Space Flight Mechanics Meeting held February 13-17, 2011, New Orleans, Louisiana (M. K. Jah, Y. Guo, A. L. Bowes, and P. C. Lai, eds.), Vol. 140 of Advances in the Astronautical Sciences, San Diego, California, American Astronautical Society, Univelt Inc., 2011, pp. 321–340.

[17] Rodney L. Anderson, "Approaching Moons from Resonance via Invariant Manifolds," 22nd AAS/AIAA Space Flight Mechanics Meeting, No. AAS 12-136, Charleston, South Carolina, January 29 - February 2 2012.

[18] R. L. Anderson, "Tour Design Using Resonant Orbit Heteroclinic Connections in Patched Circular Restricted Three-Body Problems," 23rd AAS/AIAA Space Flight Mechanics Meeting, No. AAS 13-493, Kauai, Hawaii, February 10-14 2013.

[19] R. L. Anderson, S. Campagnola, and G. Lantoine, "Broad Search for Unstable Resonant Orbits in the Planar Circular Restricted Three-Body Problem," AAS/AAIA Astrodynamics Specialist Conference, No. AAS 13-787, Hilton Head Island, South Carolina, August 11-15 2013.

[20] R. L. Anderson and M. W. Lo, "Spatial Approaches to Moons from Resonance Relative to Invariant Manifolds," Acta Astronautica, Vol. 105, 2014, pp. 355–372.

[21] W. R. Schlei, K. C. Howell, X. M. Tricoche, and C. Garth, "Enhanced Visualization and Autonomous Extraction of Poincaré Map Topology," AAS/AIAA Astrodynamics Specialist Conference, No. AAS 13-903, Hilton Head Island, South Carolina, August 11-15 2013.

[22] N. Nakhjiri and B. Villac, "Automated Stable Region Detection," AAS Spaceflight Mechanics Meeting, No. AAS 13-904, Irvine, California, February 10-14 2013.

[23] Eric Trumbauer and Benjamin Villac, "Autonomous Trajectory Redesign for Phobos Orbital Operations," 24th AAS/AIAA Space Flight Mechanics Meeting, No. AAS 14-270, Santa Fe, New Mexico, January 26-30 2014.

[24] R. L. Anderson and J. S. Parker, "Survey of Ballistic Transfers to the Lunar Surface," Journal of Guidance, Control, and Dynamics, Vol. 35, July - August 2012, pp. 1256–1267.

[25] R. L. Anderson and J. S. Parker, "Comparison of Low-Energy Lunar Transfer Trajectories to Invariant Manifolds," Celestial Mechanics and Dynamical Astronomy, Vol. 115, February 2013, pp. 311–331.

[26] J. S. Parker and R. L. Anderson, "Targeting Low-Energy Transfers to Low Lunar Orbit," Acta Astronautica, Vol. 84, March-April 2013, pp. 1–14.

[27] J. S. Parker, R. L. Anderson, and A. Peterson, "Surveying Ballistic Transfers to Low Lunar Orbit," Journal of Guidance, Control, and Dynamics, Vol. 36, No. 5, 2013, pp. 1501–1511.

[28] J. S. Parker and R. L. Anderson, Low-Energy Lunar Trajectory Design, Vol. 12 of JPL Deep Space Communications and Navigation Series. Hoboken, New Jersey: John Wiley & Sons, Inc., 1st ed., June 2014.

[29] N. Strange, D. Landau, T. McElrath, G. Lantoine, T. Lam, M. McGuire, L. Burke, M. Martini, J. Dankanish, "Overview of Mission Design for NASA Asteroid Redirect Robotic Mission Concept," 33rd International Electric Propulsion Conference, No. IPEC-2013-321, Washington, DC, October 6-10 2013.

[30] D. M. Reeves, B. J. Naasz, C. A. Wright, and A. J. Pini, "Proximity Operations for the Robotic Boulder Capture Option for the Asteroid Redirect Mission," AIAA SPACE 2014 Conference and Exposition, No. AIAA 2014-4433, San Diego, California, August 4-7 2014.

[31] J. R. Brophy, L. Friedman, N. J. Strange, T. A. Prince, D. Landau, T. Jones, R. Schweickart, C. Lewicki,M. Elvis,D. Manzella, "Synergies of Robotic Asteroid Redirection Technologies and Human Space Exploration," 65th International Astronautical Congress, No. IAC-14.A5.3-B3.6.7,x26388, Toronto, Canada, 2014.

[32] D. J. Scheeres, R. Gaskell, S. Abe, O. Barnouin-Jha, T. Hashimoto, J. Kawaguchi, T. Kubota, J. Saito, M. Yoshikawa, N. Hirata, T. Mukai, M. Ishiguro, T. Kominato, K. Shirakawa, and M. Uo, "The Actual Dynamical Environment About Itokawa," AIAA/AAS Astrodynamics Specialist Conference and Exhibit, No. AIAA 2006-6661, Keystone, Colorado, August 21-24 2006.

[33] M. W. Busch, S. J. Ostro, L. A. M. Benner, M. Brozovic, J. D. Giorgini, J. S. Jao, D. J. Scheeres, C. Magri, M. C. Nolan, E. S. Howell, P. A. Taylor, J.-L. Margot, and W. Brisken, "Radar Observations and the Shape of Near-Earth Asteroid 2008 EV5," Icarus, Vol. 212, January 2011, pp. 649–660.

[34] G. R. H. Pedro J. Llnanos, Jame K. Miller 2014 Spaceflight Mechanics Meeting, No. AAS 14-360, 2014.

[35] D. J. S. Robert A. Werner, "Exterior gravitation of a polyhedron derived and compared with harmonic and mascon gravitation representations of asteroid 4769 Castalia," Celestial Mechanics and Dynamical Astronomy, Vol. 65, 1996/1997, pp. 313–344.

[36] B. V. Andrew Colombi, Anil Hirani, "Adaptive Gravitational Force Representation for Fast Trajectory Propagation Near Small Bodies," Journal of Guidance, Control, and Dynamics, Vol. 31, No. 4, 2008, pp. 1041–1051.

[37] D. A. Vallado, Fundamentals of Astrodynamics and Applications. Microcosm Press, 2007.

[38] E. Doedel, "AUTO software for continuation and bifurcation problems in ordinary differential equations," "http://indy.cs.concordia.ca/auto/".

[39] A. E. Roy and M. W. Ovenden, "On the Occurrence of Commensurable Mean Motions in the Solar System. The Mirror Theorem," Monthly Notices of the Royal Astronomical Society, Vol. 115, No. 3, 1955, pp. 296–309.

[40] A. Miele, "Theorem of Image Trajectories in the Earth-Moon Space," Astronautica Acta, Vol. 6, No. 51, 1960, pp. 225–232.

[41] K. C. Howell and J. V. Breakwell, "Three-Dimensional, Periodic, 'Halo' Orbits," Celestial Mechanics, Vol. 32, January 1984, pp. 53–71.

[42] B. G. Marchand, K. C. Howell, and R. S. Wilson, "Improved Corrections Process for Constrained Trajectory Design in the n-Body Problem," Journal of Spacecraft and Rockets, Vol. 44, July-August 2007, pp. 884–894.

[43] N. Nakhjiri and B. Villac, "Automated stable region generation, detection, and representation for applications to mission design," Celestial Mechanics and Dynamical Astronomy, Published online 25 June 2015.

[44] N. Nilsson, Artificial Intelligence: A New Synthesis. San Francisco: Morgan Kaufmann, 1998.

[45] I. Bürk, "Spectral Clustering," Bachelor thesis, Universität Stuttgart, 2012. Available online on Matlab central (file ID File ID: #34412).

[46] P. H. Smith, B. Rizk, E. Kinney-Spano, , C. Fellows, C. d'Aubigny, and C. Merrill, "The OSIRIS-REx Camera Suite (OCAMS)," 44th Lunar and Planetary Science Conference, The Woodlands, TX, March 18-22 2013.

[47] D. Scheeres, "Close Proximity Operations for Implementing Mitigation Strategies," 2004 Planetary Defense Conference: Protecting Earth from Asteroids, No. AIAA-2004-1445, Orange County, CA, February 23-26 2004.

[48] A. J. Pini, "Investigation of the Effect of Repeat Orbits on GRACE Gravity Recovery," Master's thesis, The University of Texas at Austin, 2012.

[49] B. Gunter, Computational Methods and Processing Strategies for Estimating Earth's Gravity Field. PhD thesis, The University of Texas at Austin, 2004.

[50] R. Gaskell, O. Barnouin-Jha, D. Scheeres, A. Konopliv, T. Mukai, S. Abe, J. Saito, M. Ishiguro, T. Kubota, T. Hashimoto, J. Kawaguchi, M. Yoshikawa, K. Shirakawa, T. Kominato, N. Hirata, and H. Demura, "Characterizing and Navigating Small Bodies with Imaging Data," Meteorics and Planetary Science, Vol. 43, July 2008, pp. 1049–1061.